Characterization of Monolayer Formation on Aluminum-Doped Zinc Oxide Thin Films

Crissy L. Rhodes,† Simon Lappi,† Daniel Fischer,§ Sharadha Sambasivan,§ Jan Genzer,‡ and Stefan Franzen*,†

Department of Chemistry, North Carolina State University, Raleigh, North Carolina 27695-8204, Department of Chemical & Biomolecular Engineering, North Carolina State University, Raleigh, North Carolina 27695-7905, and National Institute of Standards and Technology, Gaithersburg, Maryland 20899

Received June 12, 2007. In Final Form: October 1, 2007

The optical and electronic properties of aluminum-doped zinc oxide (AZO) thin films on a glass substrate are investigated experimentally and theoretically. Optical studies with coupling in the Kretschmann configuration reveal an angle-dependent plasma frequency in the mid-IR for p-polarized radiation, suggestive of the detection of a Drude plasma frequency. These studies are complemented by oxygen depletion density functional theory studies for the calculation of the charge carrier concentration and plasma frequency for bulk AZO. In addition, we report on the optical and physical properties of thin film adlayers of *n*-hexadecanethiol (HDT) and *n*-octadecanethiol (ODT) self-assembled monolayers (SAMs) on AZO surfaces using reflectance FTIR spectroscopy, X-ray photoelectron spectroscopy (XPS), contact angle, and near-edge X-ray absorption fine structure (NEXAFS) spectroscopy. Our characterization of the SAM deposition onto the AZO thin film reveals a range of possible applications for this conducting metal oxide.

Introduction

The development of biosensing applications of thin films has been dependent upon the development of robust self-assembled monolayers (SAMs) for the attachment of biomolecules to such surfaces. For this reason, there has been enormous interest in SAM technology in the past few years.[1−6] The applications of SAM technology have focused primarily on gold as the substrate using a wide range of techniques, including electrochemistry, surface plasmon resonance (SPR), scanning tunneling microscopy, reflectance Fourier transform infrared (FTIR) spectroscopy, and X-ray photoelectron spectroscopy (XPS).[7−13] These studies have shown that alkane thiolates produce stable reproducible monolayers on gold substrates.[6,13−16] Conducting metal oxides present a number of interesting properties, such as optical transparency, a wide range of surface-attachment chemistries, stability at high voltage, and stability in the presence of ions that solubilize metals, such as gold. The stability of conducting metal oxide films to dissolution by acid is an important factor that must be considered to be a potential disadvantage in some applications. Self-assembled monolayers can serve to protect the metal oxide surface from attack by acid. Moreover, a fundamental study of the properties of self-assembled monolayers on optically transparent substrates is a key step in the development of multiplexing of sensing techniques, such as optical spectroscopy or microscopy coupled to electrochemistry. The potential advantage of dual sensing capabilities and tunability requires the study of both the SAMs and optical properties of the thin layer conducting metal oxides.

Transparent conducting metal oxides (TCOs) are materials that are transparent in the visible region and reflecting in the infrared region of the electromagnetic spectrum.[17] These materials have been used widely in optoelectrical devices such as solar cells and flat panel displays because of the need for high electrical conductivity paired with high transmittance in the visible region.[18] Indium tin oxide and fluorine-doped tin oxide are two such materials that have been widely studied.[19−21] Recently, indium tin oxide (ITO) has been shown to provide other novel applications

* Author to whom correspondence should be addressed. E-mail: stefan_franzen@ncsu.edu. Phone: (919) 515-8915. Fax: (919) 515-8909.
† Department of Chemistry, North Carolina State University.
‡ Department of Chemical & Biomolecular Engineering, North Carolina State University.
§ National Institute of Standards and Technology.

(1) Boozer, C.; Chen, S. F.; Jiang, S. Y. *Langmuir* **2006**, *22*, 4694−4698.
(2) Hoque, E.; DeRose, J. A.; Hoffmann, P.; Mathieu, H. J.; Bhushan, B.; Cichomski, M. *J. Chem. Phys.* **2006**, *124*.
(3) Lee, S.; Park, J.; Ragan, R.; Kim, S.; Lee, Z.; Lim, D. K.; Ohlberg, D. A. A. *J. Am. Chem. Soc.* **2006**, *128*, 5745−5750.
(4) Schreiber, F. *Prog. Surf. Sci.* **2000**, *65*, 151−256.
(5) Ulman, A. *Chem. Rev.* **1996**, *96*, 1533−1554.
(6) Ulman, A. *Thin Films: Self-assembled Monolayers of Thiols (Thin Films)*; Academic Press: New York, 1998.
(7) Kitagawa, K.; Morita, T.; Kimura, S. *J. Phys. Chem. B* **2004**, *108*, 15090−15095.
(8) Liu, Y. J.; Kalambur, A. T.; Rabolt, J. F.; Chase, D. B. *Langmuir* **2004**, *20*, 816−822.
(9) Kontturi, E.; Thune, P. C.; Niemantsverdriet, J. W. *Langmuir* **2003**, *19*, 5735−5741.
(10) Yuge, R.; Miyazaki, A.; Enoki, T.; Tamada, K.; Nakamura, F.; Hara, M. *J. Phys. Chem. B* **2002**, *106*, 6894−6901.
(11) Han, S. W.; Joo, S. W.; Ha, T. H.; Kim, Y.; Kim, K. *J. Phys. Chem. B* **2000**, *104*, 11987−11995.
(12) Corn, R. M.; Hurtt, G.; Smith, E.; Nelson, B.; Grimsrud, T. Surface plasmon resonance imaging measurements of DNA, RNA, and protein adsorption onto DNA monolayer arrays. *Abstr. Pap. Am. Chem. Soc.* **2000**, *220*, U272−U272.
(13) Davis, F.; Higson, S. P. J. *Biosens. Bioelectron.* **2005**, 1−20.
(14) Bain, C. D.; Evall, J.; Whitesides, G. M. *J. Am. Chem. Soc.* **1989**, *111*, 7155−7164.
(15) Bain, C. D.; Biebuyck, H. A.; Whitesides, G. M. *Langmuir* **1989**, *5*, 723−727.
(16) Nuzzo, R. G.; Zegarski, B. R.; Dubois, L. H. Fundamental-Studies of the Chemisorption of Adsorbates on Well-Defined Organic-Surfaces. *J. Electrochem. Soc.* **1987**, C110−C110.
(17) Lam, C. N. C.; Wu, R.; Li, D.; Hair, M. L.; Neumann, A. W. *Adv. Colloid Interface Sci.* **2002**, *96*, 169−191.
(18) Suh, K. J.; Okada, H.; Wakahara, A.; Kim, H. J.; Chang, H. J.; Yoshida, A. Proceedings of the 11th Asian Pacific Conference on Nondestructive Testing, Jeju Island, Korea, November 3−7, 2003. Transparent Conducting ZnO Films on Polymer Substrates by Pulsed Laser Deposition. In *Advances in Nondestructive Evaluation*; Lee, S.-S., Yoon, D.-J., Lee, J.-H., Lee, S., Eds.; Trans Tech Publications: Uetikon-Zuerich, Switzerland, 2004; Vol. 270−273, Pts. 1−3, pp 878−883.
(19) Bhaumik, S.; Barua, A. K. *Jpn. J. Appl. Phys, Part 1* **2003**, *42*, 3619−3620.
(20) Brewer, S.; Franzen, S. Optical properties of indium tin oxide and fluorine doped tin oxide surfaces: correlation of plasmon frequency, reflectivity and skin depth with conductivity. *J. Alloys Compd.* **2002**, *338*, 73−79.
(21) Lowe, L. B.; Brewer, S. H.; Kramer, S.; Fuierer, R. R.; Qian, G. G.; Agbasi-Porter, C. O.; Moses, S.; Franzen, S.; Feldheim, D. L. *J. Am. Chem. Soc.* **2003**, *125*, 14258−14259.

10.1021/la701741m CCC: $40.75 © 2008 American Chemical Society
Published on Web 12/11/2007

such as thermographic sensing, photothermal electrochemistry, and photoelectrochemistry, which are important in the development of biosensing applications.[20−24] A major limitation of the development of technology based on ITO is that indium is found only in minute amounts in the earth's crust and typically is extracted as a residue of ore processing to produce metals, primarily zinc.[25] Because of the prohibitive cost, availability, and environmental concerns of ITO, other materials with similar properties are being investigated for applications that require optical transparency combined with moderate conductivity.[26]

Zinc oxide (ZnO) is one alternative to ITO for conducting thin film applications. Typical ZnO films are transparent n-type conducting metal oxides. The useful electro-optical properties, stability, and band gap of ZnO arise primarily from intrinsic defects, such as oxygen vacancies and zinc interstitials. For instance, in the presence of hydrogen plasma, chemisorbed oxygen can form a protective layer of surface hydroxyls (−OH) that resists reduction of the thin film surface.[27] Because the conductivity of the zinc interstitials within pure ZnO is not enough for use as transparent semiconductors, dopants are added. The addition of a higher valence element such as an aluminum dopant (2−5%) to ZnO increases the conductivity by the replacement of the Zn^{+2} ions with Al^{+3}.[17] Additionally, the conductivity is highly dependent on the deposition and postdeposition parameters, which permit either the desorption or absorption of oxygen in the film; thus, both routes of increasing conductivity are important areas of research.[28−31] ZnO films have previously shown application in the areas of photosensors,[32] solar cells,[33] and nanotechnology applications.[34−36]

The resulting aluminum-doped zinc oxide (AZO) thin films are wide-band-gap (3.4 eV) transparent conducting metal oxides that present numerous advantages over traditional transparent conductive oxides (TCOs). Unlike indium tin oxide (ITO) and cadmium tin oxide (CTO), AZO is nontoxic, relatively inexpensive, stable in a hydrogen plasma atmosphere, and requires lower deposition temperatures. Yet, it still maintains the characteristic properties of ITO and CTO thin films by exhibiting high optical transparency in the visible region and low electrical resistance.[37−40] AZO films have been prepared by spray pyrolysis (SP),[18] a sol−gel method,[41] reactive and nonreactive radio frequency magnetron sputtering,[42] pulsed magnetron sputtering,[43] and pulsed laser deposition.[18] The resulting hexagonal close-packed structures are highly oriented with a *c* axis normal to the glass substrate with crystalline faces of (002) and (101).[44−46]

As an alternate biosensing substrate, AZO requires further investigation into the various sensing properties, specifically, spectroscopic qualities and monolayer formation. The optical properties and electrical conductivity are similar to those of ITO, thus similar sensing characteristics may be apparent in AZO. Observed reflectivity changes as a result of plasmon oscillations have been demonstrated in ITO by FTIR and SPR spectroscopy.[23,47,48] Therefore, similar investigations are warranted in AZO. In addition, studies of SAM formation on conducting metal oxides have also been previously described in the literature for TCOs such as ITO and CTO.[22,47] Herein, we report the deposition of *n*-hexadecanethiol- and *n*-octadecanethiol-based SAMs onto the surface of a 2% aluminum-doped zinc oxide thin film. Reflectance infrared spectroscopy, X-ray photoelectron spectroscopy (XPS), contact angle, and near-edge X-ray fine structure spectroscopy (NEXAFS) are used to characterize SAM formation. These studies are complemented by density functional theory (DFT) calculations of the charge carrier concentration and the plasma frequency of oxygen-depleted substrates to increase our understanding of the material properties of the AZO.

Materials and Methods

Chemicals and Substrates. *n*-Hexadecanethiol (HDT) and *n*-octadecanethiol (ODT) were obtained from Sigma-Aldrich and used as received. Absolute ethanol was used as received from Aaper Alcohol and Chemical Co. The gold electrodes were obtained from Evaporated Metal Films, Inc.

Aluminum-Doped Zinc Oxide Tin Oxide Film Preparation. Aluminum-doped zinc oxide (AZO) electrodes were fabricated by the National Renewable Energy Laboratory (NREL) at room temperature by rf sputtering with the MRC 603 side/vertical sputter system using a 5 in. × 15 in. (nominal) Planar Magnetron ceramic target with pure argon flow of 50 sccm. The film thickness was determined by a stylus profilometer (Dektak3). The carrier concentration and electron mobility were measured using Hall effect measurements (van der Pauw technique, BioRad model HL5500). The composition of the films was analyzed by electron probe microanalysis (EPMA, JEOL 8900 Electron Microprobe), and crystal properties were assessed using X-ray diffraction (XRD, Sintag model PTS). Under 5 mTorr pressure deposition, the AZO thin films were determined to have a thickness of 120 nm. The substrate for the AZO electrodes was 0.5 mm Corning 1737 borosilicate glass.

Deposition on Aluminum-Doped Zinc Oxide Thin Films. The AZO electrodes were cleaned via 20 min of UV ozonolysis (model number 42, Jelight Co. Inc.) to yield a clean hydrophilic surface and remove any adventitious carbon present.[48] The clean AZO electrode was subsequently immersed in the deposition solution of ODT or HDT (10 mM) in absolute ethanol for up to 30 min. The electrodes were rinsed with 95% ethanol, followed by drying with N_2 gas.

(22) Brewer, S. H.; Brown, D. A.; Franzen, S. *Langmuir* **2002**, *18*, 6857−6865.
(23) Appleyard, S.; Day, S.; Pickford, R.; Willis, M. *J. Mater. Chem.* **2000**, *10*, 169−173.
(24) Zotti, G.; Schiavon, G.; Zecchin, S.; Berlin, A.; Pagani, G. *Langmuir* **1998**, *14*, 1728−1733.
(25) Coutts, T. J. *Sol. Cells* **1981**, *3*, 375−386.
(26) Ginley, D.; Roy, B.; Ode, A.; Warmsingh, C.; Yoshida, Y.; Parilla, P.; Teplin, C.; Kaydanova, T.; Miedaner, A.; Curtis, C.; Martinson, A.; Coutts, T.; Readey, D.; Hosono, H.; Perkins, J. *Thin Solid Films* **2003,** *445*, 193−198.
(27) Major, S.; Chopra, K. L. *Sol. Energy Mater.* **1988**, *17*, 319−327.
(28) Jeong, W. J.; Park, G. C. *Sol. Energy Mater. Sol. Cells* **2001**, *65*, 37−45.
(29) Jeong, W. J.; Kim, S. K.; Park, G. C. *Thin Solid Films* **2006**, *506*, 180−183.
(30) Kang, D. J.; Kim, J. S.; Jeong, S. W.; Roh, Y.; Jeong, S. H.; Boo, J. H. *Thin Solid Films* **2005**, *475*, 160−165.
(31) Nunes, P.; Fortunato, E.; Martins, R. *Thin Solid Films* **2001**, *383*, 277−280.
(32) Nikitin, S. E.; Nikolaev, Y. A.; Polushina, I. K.; Rud, V. Y.; Rud, Y. V.; Terukov, E. I. *Semiconductors* **2003**, *37*, 1291−1295.
(33) Song, D. Y.; Aberle, A. G.; Xia, J. *Appl. Surf. Sci.* **2002**, *195*, 291−296.
(34) Jeong, M. C.; Oh, B. Y.; Nam, O. H.; Kim, T.; Myoung, J. M. *Nanotechnology* **2006**, *17*, 526−530.
(35) Jeong, J. S.; Lee, J. Y.; Cho, J. H.; Suh, H. J.; Lee, C. J. *Chem. Mater.* **2005**, *17*, 2752−2756.
(36) Suh, H. W.; Kim, G. Y.; Jung, Y. S.; Choi, W. K.; Byun, D. *J. Appl. Phys.* **2005**, *97*, 044305-1 to 044305-6.
(37) Chang, J. F.; Lin, W. C.; Hon, M. H. *Appl. Surf. Sci.* **2001**, *183*, 18−25.
(38) Chang, J. F.; Hon, M. H. *Thin Solid Films* **2001**, *386*, 79−86.
(39) El Hichou, A.; Addou, M.; Bougrine, A.; Dounia, R.; Ebothe, J.; Troyon, M.; Amrani, M. *Mater. Chem. Phys.* **2004**, *83*, 43−47.
(40) El Hichou, A.; Addou, M.; Ebothe, J.; Troyon, M. *J. Lumin.* **2005**, *113*, 183−190.
(41) Paul, G. K.; Bandyopadhyay, S.; Sen, S. K.; Sen, S. *Mater. Chem. Phys.* **2003**, *79*, 71−75.
(42) Das, R.; Ray, S. *J. Phys. D: Appl. Phys.* **2003**, *36*, 152−155.
(43) Kelly, P. J.; Hisek, J.; Zhou, Y.; Pilkington, R. D.; Arnell, R. D. *Surf. Eng.* **2004**, *20*, 157−162.
(44) Hong, R. J.; Helming, K.; Jiang, X.; Szyszka, B. *Appl. Surf. Sci.* **2004**, *226*, 378−386.
(45) Hong, R. J.; Jiang, X.; Szyszka, B.; Sittinger, V.; Xu, S. H.; Werner, W.; Heide, G. *J. Cryst. Growth* **2004**, *260*, 606−606.
(46) Czternastek, H. *Opto-Electron. Rev.* **2004**, *12*, 49−52.
(47) Rhodes, C. L.; Brewer, S. H.; Folmer, J.; Franzen, S. *Thin Solid Films*, in press, available on-line August 24, 2007.
(48) Tominaga, M.; Hirata, N.; Taniguchi, I. *Electrochem. Commun.* **2005**, *7*, 1423−1428.

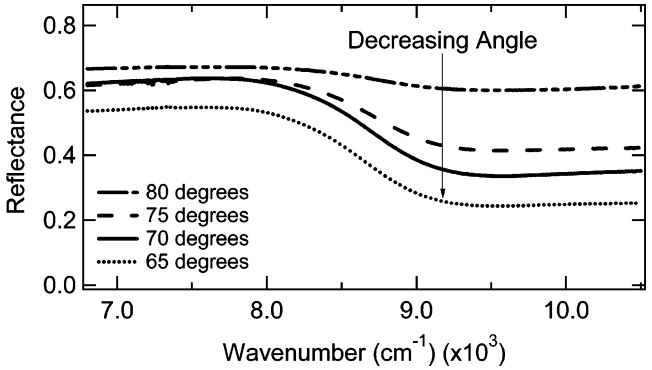


Figure 1. Experimental variable angle reflectance FTIR spectra of a thin film of AZO (80 Ω/sq, 4.7 × 1020 e/cm) on a glass substrate relative to a gold surface in the mid-IR region for angles of incidence ranging from 65 to 80° with p-polarized light.

Reflectance FTIR Spectroscopy. All reflectance spectra were collected with a Digilab FTS-3000 Fourier transform infrared (FTIR) spectrometer using a Varian Universal variable grazing angle reflectance attachment. An infrared polarizer was used to obtain p-(vertically) polarized light. The infrared light is generated by a globar source and is then passed through a potassium bromide (KBr) beamsplitter and focused onto the photodiode of a liquid-nitrogen-cooled, narrow band mercury−cadmium−telluride (MCT/A) linearized detector with a normal spectral response of 650−7000 cm^{-1}. The angle of incidence used was 70° with respect to the surface normal for the alkanthiolate thin film reflectance studies. To obtain the AZO thin film reflectance spectra at multiple angles of incidence, a ratio of the single-beam spectra of the metal oxide thin film on the glass substrate to the single-beam spectra of a gold surface was used. The IR spectra presented are an average of 32 scans taken at a resolution of 2 cm^{-1}. The spectra of the thiolated adlayers on the AZO electrode were obtained by taking a ratio of the single-beam spectra of the p-polarized spectra of the deposited material (HDT or ODT) on AZO to the s-polarized spectra of the same aluminum-doped zinc oxide thin film. All SAM IR spectra are an average of 256 scans at a resolution of 2 cm^{-1}.

X-ray Photoelectron Spectroscopy. XPS spectra were recorded on a VG CLAM II surface analysis system (100 mm mean radius) with Mg Kα X-rays ($h\nu = 1253.6$ eV, takeoff angle = 90°) operated at 13 kV and 20 mA emission current. The elemental scans had a resolution of 1 eV as determined from the full width at half-maximum (fwhm) of a gold $4f_{7/2}$ spectral peak with three scans performed for zinc and seven scans performed for sulfur.

Contact Angle Measurements. Contact angle experiments were performed using a Ramé-Hart contact angle goniometer (model 100-00) equipped with a CCD camera and analyzed with Ramé-Hart software. Advancing contact angles were measured by depositing 8 μL of deionized (DI) water on the sample surface, and receding angles were measured after removing 4 μL of water from the deposited drop. These operations were repeated three times on three different repetitions of each thiolated sample, and the results were averaged.

Near-Edge X-ray Fine Structure Spectroscopy (NEXAFS). The NEXAFS experiments were performed at the NIST/DOW soft X-ray materials characterization facility located at the U7A beamline at the National Synchrotron Light Source at Brookhaven National Laboratory with a resolution of ~0.15 eV at the carbon K edge. The monochromator energy resolution was calibrated by setting a graphite carbon K-edge transition of C(1s) → π* equal to 285.35 eV.[49] The partial electron yield (PEY) signal was collected with a channeltron electron multiplier (50-mm-diameter entrance cone) with an adjustable entrance grid bias (EGB) set to EGB = −150 V, allowing the rejection of low-energy inelastic auger electrons from below the surface. To account for fluctuations in the beamline X-ray intensity,

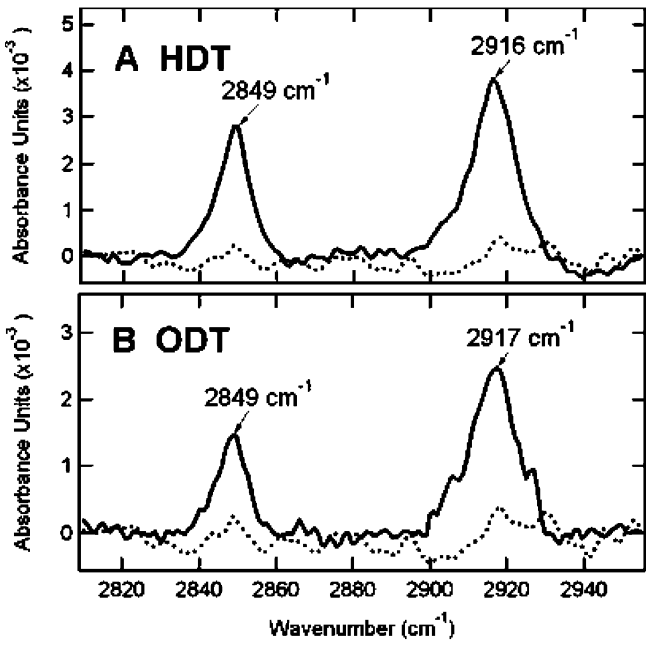


Figure 2. (A, B) Baseline-corrected reflectance FTIR spectra obtained from a ratio of p-polarized light of 1-hexadecanethiol and 1-octadecanethiol on AZO to s-polarized light of a bare AZO slide. The spectra shown are for an angle of incidence of 70°. The reference AZO (---) was cleaned via 20 min of UVO. The adlayer (−) deposition time was for 30 and 15 min for the hexadecanthiol (A) and octadecanethiol (B) solutions, respectively.

the NEXAFS spectra were normalized with the incident beam intensity (I_o) from the photoyield of a clean in situ gold-coated grid. A computer-controlled stepping motor directed the orientation of the sample holder with respect to the polarization vector of the incoming X-ray beam for incident angles between the X-ray beam and the sample surface of 30° (near glancing geometry) to 90° (normal geometry). The cartoon in Figure 4A and B depicts the schematic of the performed NEXAFS experiments. The NEXAFS spectra were collected in the PEY mode for the analysis of Auger electrons with photon energy ranging from 240 to 400 eV. The PEY NEXAFS spectra were normalized by adjusting the preedge and postedge signals respectively to 0 and 1.[50]

Tilt Angle Calculations. Tilt angle calculations were performed by the method reported by Outka et.al.[51] The intensity of the NEXAFS spectrum represents a molecular orbital transitioning from the bonding to the antibonding state of a X−Y σ bond (1s → σ_{X-Y}*) and is expressed by eq 1[51]

$$I_{X-Y} = A[PI^{\parallel}_{X-Y} + (1 - P)I^{\perp}_{X-Y}] \quad (1)$$

where A is a prefactor constant, P is the polarization factor of the X-ray beam, and $I^{\parallel}_{X-Y}$ and $I^{\perp}_{X-Y}$ give the resonance intensities of the parallel and perpendicular components of the X-ray beam **E** vector, respectively. The expressions for $I^{\parallel}_{X-Y}$ and $I^{\perp}_{X-Y}$ are given by eqs 2 and 3[51]

$$I^{\parallel}_{X-Y} = B\left[\cos^2(\theta)\cos^2(\alpha_{X-Y}) + \frac{1}{2}\sin^2(\theta)\sin^2(\alpha_{X-Y})\right] \quad (2)$$

$$I^{\perp}_{X-Y} = \frac{B}{2}\sin^2(\alpha_{X-Y}) \quad (3)$$

where B is a prefactor that is a function of the bond absorption cross section and instrumental parameters, θ is the angle between the substrate normal and the **E** (electric field vector) of the polarized

(49) Furukawa, M.; Fujisawa, H.; Katano, S.; Ogasawara, H.; Kim, Y.; Komeda, T.; Nilsson, A.; Kawai, M. *Surf. Sci.* **2003**, *532*, 261−266.

(50) Stohr, J. *NEXAFS Spectroscopy*; Springer: Berlin, 1992.

(51) Outka, D. A.; Stohr, J.; Rabe, J. P.; Swalen, J. D. *J. Chem. Phys.* **1988**, *88*, 4076−4087.

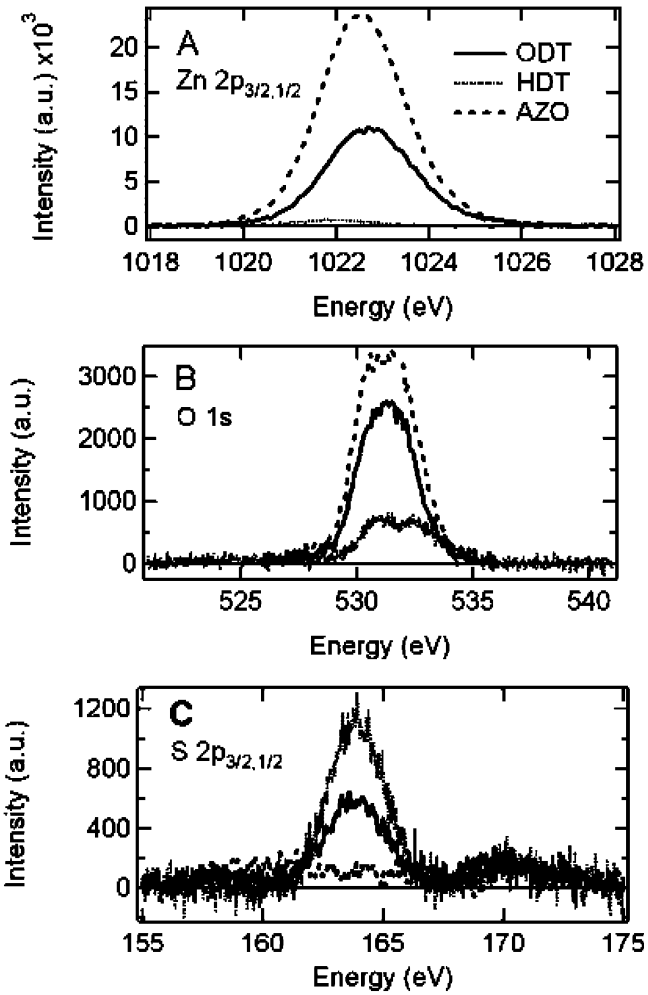


Figure 3. (A−C) XPS spectra corresponding to an adlayer of 1-hexadecanethiol (···) and 1-octadeanethiol (−) on AZO compared to a bare reference AZO (---). (A) Zinc $2p_{3/2,1/2}$ region. (B) Oxygen 1s region. (C) Sulfur $2p_{3/2,1/2}$ region.

X-ray beam, and α_{X-Y} is the angle between the surface normal and the $X-Y$ bond of the antibonding orbital. Equation 4 relates the combination of eqs 1−3

$$I_{X-Y} = C\left[P\left(\cos^2(\theta)\cos^2(\alpha_{X-Y}) + \frac{1}{2}\sin^2(\theta)\sin^2(\alpha_{X-Y})\right) + \frac{(1-P)}{2}\sin^2(\alpha_{X-Y})\right] \quad (4)$$

where C is a constant.

The tilt angle and orientation of the monolayer alkane chain are calculated using the "tilted chain" model related by Stöhr et al.[5052] where α_{C-C} and α_{C-H} are equated to the tilt angle and bond angles of the C−H backbone are assumed as shown in eqs 5 and 6

$$\alpha_{C-C} = \arcsin\left[\sqrt{\frac{1+\cos(\delta_{C-C-C})\cos(2\tau)}{2}}\right] \quad (5)$$

$$\alpha_{C-H} = \arcsin\left[\sqrt{1-\frac{\sin^2(\tau)}{1+\tan^2\left(\frac{\delta_{H-C-H}}{2}\right)}}\right] \quad (6)$$

where δ_{C-C-C} and δ_{H-C-H} are the assumed bond angle of 115° between neighboring carbon atoms[51] and the bond angle of 110° of the hydrogen−carbon−hydrogen sequence,[51] respectively, and τ is the tilt angle of the chain with respect to the surface normal.

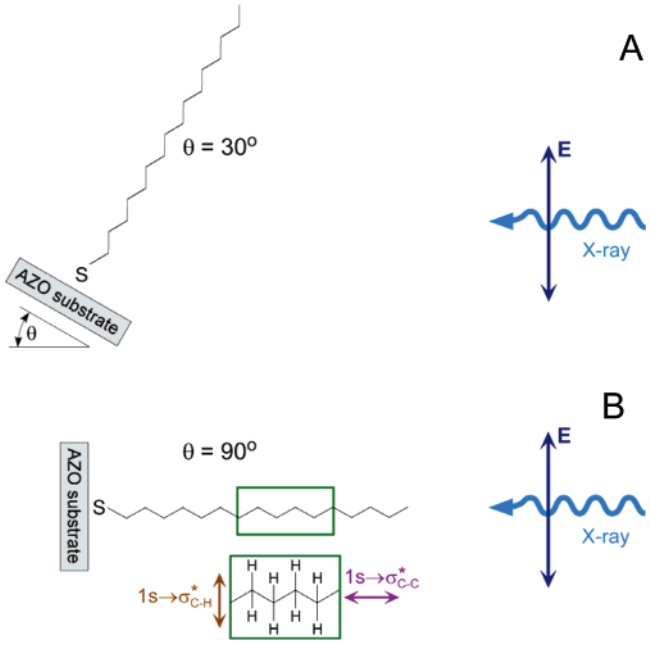


Figure 4. (A, B) Illustration of the relationship between the electric vector of the X-ray beam and the monolayer orientation on the AZO thin film. The sample geometry is depicted with photon angles of incidence of 30 and 90°, respectively. (A) The 30° geometry. (B) The 90° geometry. The orientation of the antibonding orbitals corresponding to the C−H and C−C bonds is shown in the inset

A comparison of the combination of eqs 4 and 5 of the calculated I_{C-C} to the experimental data leads to modeling of the tilt angle (τ) as the value of the constant C in eq 4 is adjusted until an adequate fit is obtained. In an analogous fashion, the tilt angle can be calculated by a comparison of the I_{C-H} experimental data to the computed intensities, eqs 4 and 6, and adjusting the constant C for an optimal fit. The reported tilt angles of the hydrocarbon chains represent an average over the two tilt chain angles calculated by the different approaches using a comparison with both the I_{C-H} and I_{C-C} experimental and computed values.

Density Functional Theory Calculations. The single-point energy calculation of the molecule was carried out with the use of quantum chemical software DMol3 (Accelrys, Inc.).[53] Density functional theory calculations were performed on an aluminum-doped zinc oxide unit cell containing 32 hexagonal formula units that comprise a total of 64 atoms with an overall orthorhombic structure. The unit cell parameters for this orthorhombic cell (a = 6.50 Å, b = 11.26 Å, and c = 10.41 Å) were expanded to find the unit cell parameters of minimum energy. The equilibrium geometry was found at 1.07a, 1.07b, and 1.07c (details in Supporting Information). This $Zn_{32}O_{32}$ orthorhombic cell (a = 6.95 Å, b = 12.05 Å, and c = 11.14 Å) was used to study oxygen depletion in the n-type conduction mechanism as previously described for cadmium tin oxide and doping.[47] Oxygen depletion stoichiometries ranging from $Zn_{32}O_{32}$ to $Zn_{32}O_{26}$ were studied by random removal of oxygen atoms from random positions as previously described[47] for undoped and aluminum-doped (1.6, 3.1, and 4.7%) zinc oxide structures. Periodic boundary conditions were used to determine the bulk electronic and optical properties of the metal oxide thin film. The double numerical plus p-function (DNP) basis set used was O(1s), 2(2s), 2(2p), 2(3d), Zn(4s),(4p), 2(4d) for the atoms with an atomic cutoff of 5.5 Å. The Perdew and Wang GGA functional was used for the DFT calculations.[54] The DFT calculations utilized the grand canonical ensemble approach, which allows for partial electron

(52) Stohr, J.; Outka, D. A. *Phys. Rev. B* **1987**, *36*, 7891−7905.

(53) Delley, B. *J. Chem. Phys.* **1990**, *92*, 508−517.

(54) Perdew, J. P.; Chevary, J. A.; Vosko, S. H.; Jackson, K. A.; Pederson, M. R.; Singh, D. J.; Fiolhais, C. *Phys. Rev. B* **1992**, *46*, 6671−6687.

occupation needed for charge carrier calculations.[55] In all previous calculations using this method, an effective electronic temperature of 0.02 hartree or ~6300 K has been sufficient to guarantee self-consistent field (SCF) convergence. However, AZO thin film calculations, in which a layer thin film model is used for the AZO along its 001 axis with an ethane thiolate overlayer in a $(\sqrt{3} \times 3)R30°$ hexagonal lattice, required an electronic temperature of 0.04 hartree. The molecules in the adlayer were found to have a remarkable resemblance to the adlayer on Au(111) surfaces. In that case as well, the surface can be modeled using an orthorhombic unit cell.

The number of conduction electrons was determined from the energy bands above the Fermi energy, ϵ_F, at an electronic temperature of 300 K. The charge carrier concentration value was determined by summing the electrons in the conduction band of aluminum-doped zinc oxide divided by the unit cell volume calculated from the lattice constants. The plasma frequency was determined using eq 7[56]

$$\omega_p^2 = \frac{ne^2}{m^*\epsilon_o} \tag{7}$$

where ω_p is the plasma frequency, n is the charge carrier concentration, e is the charge of a conduction electron, ϵ_o is the permittivity of space, and m^* is the effective mass of aluminum-doped zinc oxide of approximately 0.28.[57] Thus, the plasma frequency is calculated directly from first principles using the Drude free-electron model. All of the DFT calculations were performed at the high-performance computing Linux cluster at North Carolina State University.

Results and Discussion

The reflectivity of aluminum-doped zinc oxide (AZO) thin films was measured experimentally by variable-angle Fourier transform infrared (FTIR) reflectance spectroscopy. Figure 1 reveals an angle-dependent reflectance change observed at ~8500 cm^{-1}. At wavenumbers below 8500 cm^{-1}, the reflectance of the thin film varies between ~55 and 65% reflectance depending on the angle of incidence, whereas above 8500 cm^{-1} the reflectance drops to ~30% for data obtained at an angle of incidence of $\leq 70°$. The reduction in reflectance for incidence at 75 and 80° is substantially less (Figure 1). The reduction in reflectivity coincides with the plasmon resonance frequency, which is the resonant absorption frequency for the conduction electrons as described in the Drude model. Below the plasma frequency of AZO at 8500 cm^{-1}, the conduction electrons oscillate in phase with the incident radiation, which leads to reflection. When the incident radiation is matched to the resonant plasma frequency, the resonance condition leads to a sharp decrease in the reflectivity of the film. Above the plasma frequency, the AZO conduction electrons can no longer be driven in phase by the incident radiation, and electromagnetic radiation is transmitted. In sp-type conductors such as AZO, there is an increase in the optical transparency of the film at wavenumbers higher than the plasma frequency, which is due to the absence of absorption bands in this region.

Alkane thiolate SAMs on AZO films were prepared by deposition for 15 and 30 min for hexadecane thiol (HDT) and octadecane thiol (ODT), respectively. This is in contrast to the neat thiol solution and overnight deposition required to create SAMs on ITO. It is noteworthy that the conditions for the formation of SAMs on AZO are similar to those on gold surfaces. Figure 2A,B shows experimental FTIR reflectance spectra for a bare AZO thin film and an AZO thin film with a thiolate adlayer of either HDT (A) or ODT (B). The dashed line displays the bare aluminum-doped zinc oxide thin film, and the solid line reveals the spectra of the AZO with a thiolate adlayer. The vibrational symmetric and antisymmetric C−H stretching peaks are centered at 2849 and 2916 cm^{-1}, respectively. The position of these bands is indicative of an ordered adlayer on the surface. Additionally, as shown for other CMOs deposited on glass substrates,[22,58] these spectra also displayed bands from the glass substrate onto which the aluminum-doped zinc oxide was deposited with the longitudinal optical (LO) and transverse optical (TO) Si−O−Si stretching modes observed at 1248 and 1064 cm^{-1} (data not shown). The FTIR data revealed that both the HDT (16 carbons) and ODT (18 carbons) are well suited for the deposition of long-chain alkane thiolates.

Although previous studies with the deposition of HDT on ITO thin films[22] revealed analogous peak positions of the C−H stretching modes, the intensities were lower than those reported for alkanethiolate SAMs on gold, indicative of lower surface coverage for SAMs deposited on ITO than on gold. Specifically, the optical density of a SAM on an ITO substrate is typically less than 0.001 au[22] whereas thiolated SAMs on gold range from 0.002 to 0.006 au.[16,59,60] NEXAFS measurements are consistent with a lower coverage and a lower order parameter for alkanethiolate SAMs on ITO compared to those on gold.[61] However, HDT SAMs on CTO had absorbances ranging from 0.002 to 0.003.[47] For the HDT SAM on AZO, the total absorbance was in the range of 0.003 to 0.004 whereas for the ODT SAM the absorbance ranged from 0.0015 to 0.0025. In addition, the stability of the AZO thin films was tested by acquiring FTIR spectra 1 year after preparation. The thiolate SAMs appear to be stable after 1 year as evidenced by the presence of distinct C−H stretching modes although the intensity is diminished by 25−50%. Extended washing with an aqueous solvent such as ethanol for several minutes also does not destroy the SAMs as shown by the presence of the CH stretching modes in an FTIR spectrum although a slight reduction of the peak intensity occurs as well as an observed small shift in the stretching peaks (data not shown). The FTIR spectra provide qualitative data that suggest that well-ordered monolayers are formed on AZO. Although a comparison of intensities is not quantitative because of the absence of information on tilt angle and surface roughness, these data suggest that SAMs on AZO are more robust than SAMs on ITO.

X-ray photoelectron spectroscopy (XPS) was also used to confirm the presence of the thiolated adlayers. Figure 3A shows the XPS spectra of zinc $2p_{3/2}$ of bare aluminum-doped zinc oxide (dashes), an adlayer of HDT (dotted), and an adlayer of ODT (solid line) on AZO at a peak position of 1022 eV originating from the Zn^{+2} atoms in the exposed substrate. The HDT and ODT SAMs demonstrate attenuations of the zinc $2p_{3/2}$ band of 97 and 50%, respectively, which are attributable to differences in surface coverage. Figure 3B reveals the XPS spectra of oxygen for the same substrate thin films. A similar attenuation of the 1s peak of oxygen (532 eV) provides additional evidence for the formation of an adlayer on AZO and follows a similar trend with attenuations of 75 and 30% observed for the HDT and the ODT monolayer, respectively. Figure 3C reveals the sulfur $2p_{3/2,1/2}$ XPS spectra of an adlayer of both HDT and ODT on AZO using base AZO as a reference. These peaks, occurring at 162 and

(55) Mermin, N. D. *Phys. Rev. A* **1965**, *137*, 1441−1443.
(56) Wooten, F., *Optical Properties of Solids*; Academic Press: San Diego, CA, 1972.
(57) Coutts, T. J.; Wu, X.; Mulligan, W. P.; Webb, J. M. *J. Electron. Mater.* **1996**, *25*, 935−943.
(58) Brewer, S. H.; Wicaksana, D.; Maria, J. P.; Kingon, A. I.; Franzen, S. *Chem. Phys.* **2005**, *313*, 25−31.
(59) Inman, C. E.; Reed, S. M.; Hutchison, J. E. *Langmuir* **2004**, *20*, 9144−9150.
(60) Laibinis, P. E.; Whitesides, G. M.; Allara, D. L.; Tao, Y. T.; Parikh, A. N.; Nuzzo, R. G. *J. Am. Chem. Soc.* **1991**, *113*, 7152−7167.
(61) Cerruti, M. R., C.; Losego, M.; Efremenko, A.; Maria, J. P.; Fischer, D.; Feldheim, D.; Franzen, S.; Genzer, J. *J. Phys. D: Appl. Phys.* **2007**, *40*, 4212−4221.

Table 1. Advancing, Receding, and Difference Contact Angles (±SD) Measured Using Deionized Water on AZO with Hexadecanethiol (HDT) and Octadecanethiol (ODT)

SAM	advancing CA[a]	receding CA[a]	difference
hexadecanethiol	84.1 ± 12.1	73.7 ± 8.9	10.4
octadecanethiol	92.4 ± 13.0	80.8 ± 8.2	11.6

[a] Denotes the average of three samples, each with three sampling regions.

163.7 eV, appear to coalesce into one indistinct peak centered at 164 eV. This position corresponds to a sulfur signal that is intermediate for thiolates and oxidized sulfur species,[62] which is not surprising considering the possibilities for partial sulfur oxidation on a metal oxide surface. The intensity of the sulfur peak is similar to those previously reported for SAMs on cadmium tin oxide and ITO.[22,47] The intensity of the sulfur $2p_{3/2,1/2}$ XPS peak for HDT is twice as large as that for ODT, which can be attributed to the difference in coverage indicated by the FTIR data in Figure 2. The difference in the Zn $2p_{3/2,1/2}$ and O 1s XPS signals is also consistent with better coverage for the HDT layer as considered previously on gold surfaces.[16,59]

Contact angle measurements reveal information about the degree of packing of the monolayers on the surface. Ideally, a physically smooth homogeneous sample would require only a single contact angle measurement.[17] To account for chemical or physical inhomogeneties, advancing and receding contact angles are measured. The difference between these two contact angle values, known as contact angle hysteresis (CAH), reveals information about any imperfection (physical and/or chemical) in the monolayer.[63] Table 1 reveals the results ± standard deviation of the advancing and receding contact angles measured using deionized water on both hexadecanethiol (HDT) and octadecanethiol (ODT) SAMs deposited on aluminum-doped zinc oxide (AZO). The average contact angle was ∼84° for HDT and ∼92° for ODT, indicating that the surfaces are not as well packed as commonly reported for an aliphatic SAM on a CMO (>110°).[64] The CAH ranged from 8 to 17° for both types of thiols, indicating an inhomogeneous surface. Previous studies on ITO revealed a CAH of 15−20° with SAMs of thiols and carboxylic acids indicative of the greater inhomogeneity of ITO surfaces compared with that of AZO.[61]

The HDT and ODT adlayers on AZO were also investigated using near-edge X-ray absorption fine structure spectroscopy (NEXAFS), which is a surface-sensitive technique that is capable of examining the molecular organization of SAMs on substrates. In NEXAFS, core electrons from the K or L shell ground state of the SAM are excited to their corresponding antibonding molecular orbitals (σ^* or π^*) as a result of the interaction with incoming X-rays. The energy required for excitation from the carbon K shell is ∼290 eV.[65] Bonding differences are detectable as well; for instance, a C−H 1s → σ^* transition occurs at ∼287 eV whereas a C−C 1s → σ^* transition takes place at ∼294 eV.[50] As shown in the scheme in Figure 4A,B, orientation information is obtained from the angular dependence of the antibonding orbital to the polarization vector of the X-ray beam. For a well-ordered SAM, selective excitation of bonds occurs, with those bonds parallel to the electric vector of the X-ray beam displaying the highest intensity and those perpendicular to the beam polarization having no intensity. As the cartoon in Figure 4A,B depicts, for a well-ordered hydrocarbon backbone, the C−H σ bond is perpendicular to the C−C bond, and thus the 1s → σ^* transition for each of the bonds is inversely related. As the intensity of the C−H bond increases, the C−C bond decreases; the process reverses once the incident angle of the X-ray beam changes from glancing to normal incidence as shown.

NEXAFS spectra were collected at θ ranging from 30 to 90° in 10° increments, where θ is the angle of incidence between the sample normal and the electric vector of the X-ray beam. The partial electron yield (PEY) NEXAFS spectra were normalized by setting the preedge and postedge signals equal to 0 and 1, respectively, as described previously.[66] Figure 5A,B reveals the carbon K-edge PEY NEXAFS spectra collected from HDT and ODT SAM samples, respectively, deposited on 2% aluminum-doped zinc oxide thin films. The vertical dashed lines in Figure 5A,B correspond to the positions of the two primary peaks observed in the spectra. A peak observed at ∼288.2 eV is attributed to the 1s → σ^* transition to the Rydberg states of the C−H bond in a saturated alkane chain.[67] A second peak located at ∼291−293 eV is ascribed to the 1s → σ^* excitation of the C−C bond in a saturated alkane chain.[68]

The orientation of the SAM is inferred from the angle dependence of these bonds. As θ increases, the intensity of the peak corresponding to the 1s → σ^* C−H transition increases whereas the intensity of the peak indicative of the 1s → σ^* C−C transition decreases. This indicates that both of the thiolated SAMs are well-organized.[50] The difference in the molecular ordering between the HDT and ODT SAMs is not considerable, as shown by the NEXAFS difference spectra (calculated from the subtraction of the $\theta = 30°$ spectra from the $\theta = 90°$ spectra) in Figure 5C.

The magnitude of the difference intensity provides a qualitative measure of ordering in the two SAMs. The greater the peak height of the C−H and C−C peaks on the difference intensity scale, the more closely the SAM molecules are oriented toward the surface normal in the SAM. Thus relative to the HDT SAM, the molecules in ODT SAM appear to have a smaller tilt angle. The robustness of the films was examined by SAM reproduction as well as the reanalysis of samples (data not shown). Both the HDT and the ODT were exceptionally reproducible, regardless of humidity or environmental temperature. Additionally, samples analyzed 3 months after deposition showed nearly identical NEXAFS spectra (data not shown). Thus, this evidence reveals that long-chain thiolated SAMs on AZO thin films form both well-organized and robust SAMs.

Figure 6A,B relates the intensity of the NEXAFS spectra for the two specific peaks of C−H (∼288 eV, square symbol) and C−C (∼294 eV, triangle symbol) to $\sin^2\theta$. This type of plot is another qualitative indicator of the ordering of the thiolated monolayers. A steady decrease in the intensity of the C−C peaks in relation to the steady increase shown in the intensity of the C−H peaks is indicative of ordering of the SAMs. More detailed information about chain tilt can be obtained by performing an analysis using the method described previously by Outka et al.,[51] as detailed in the Materials and Methods section. The tilt angle values were determined from a comparison of the experimental and calculated intensities of the C−H and C−C peaks at different angles of incidence. Table 2 details the tilt angle values defined

(62) Petrovykh, D. Y.; Kimura−Suda, H.; Opdahl, A.; Richter, L. J.; Tarlov, M. J.; Whitman, L. J. *Langmuir* **2006**, *22*, 2578−2587.
(63) Fadeev, A. Y.; McCarthy, T. J. *Langmuir* **1999**, *15*, 3759−3766.
(64) Yan, C.; Zharnikov, M.; Golzhauser, A.; Grunze, M. *Langmuir* **2000**, *16*, 6208−6215.
(65) Ade, H. U. S. G. *Chemical Applications of Synchrotron Radiation*; World Scientific Publishing: Singapore, 2002; Vol. 12, pp 285−355.
(66) Fischer, D.; Efimenko, K.; Bhat, R.; Sambasivan, S.; Genzer, J. *Macromol. Rapid Commun.* **2004**, *25*, 141−149.
(67) Bagus, P. S.; Weiss, K.; Schertel, A.; Woll, C.; Braun, W.; Hellwig, C.; Jung, C. *Chem. Phys. Lett.* **1996**, *248*, 129−135.
(68) Stohr, J.; Outka, D. A.; Baberschke, K.; Arvanitis, D.; Horsley, J. A. *Phys. Rev. B* **1987**, *36*, 2976−2979.

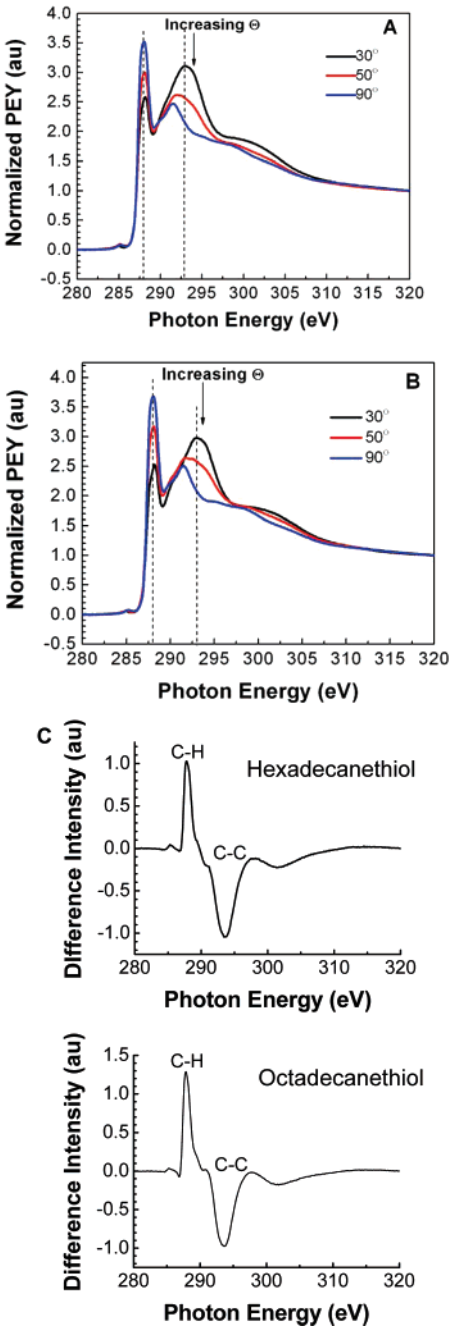


Figure 5. (A−C) Normalized carbon K-edge PEY NEXAFS spectra of a monolayer of 1-hexadecanethiol (A) and 1-octadeanethiol (B) on AZO collected at θ from 30 to 90° in increments of 10° where θ is the angle of incidence between the sample and X-ray beam. The vertical dashed lines denote the $1\sigma \rightarrow \sigma^*$ transition for C−H and C−C at 288 and 291 eV, respectively. (C) Difference spectra obtained by subtracting the intensity of the 30° angle PEY NEXAFS spectrum from the PEY NEXAFS spectrum taken at 90°.

as the angle between the surface normal and the alkyl chain in the SAM. As shown, the average tilt angle was ∼40° for HDT and ∼35° for ODT. These values are in close agreement with the reported tilt angle of 35° for thiolates deposited on clean gold surfaces,[69] which is indicative of well-organized thiolated SAMs formed on AZO that are similar to those found on gold. The individual tilt angles of each of the bonds were ∼10° different. We attribute this behavior to the approximations invoked in the "titled chain" model.[50,51] The slight difference between the tilt

(69) Yan, C.; Golzhauser, A.; Grunze, M.; Woll, C. *Langmuir* **1999**, *15*, 2414−2419.

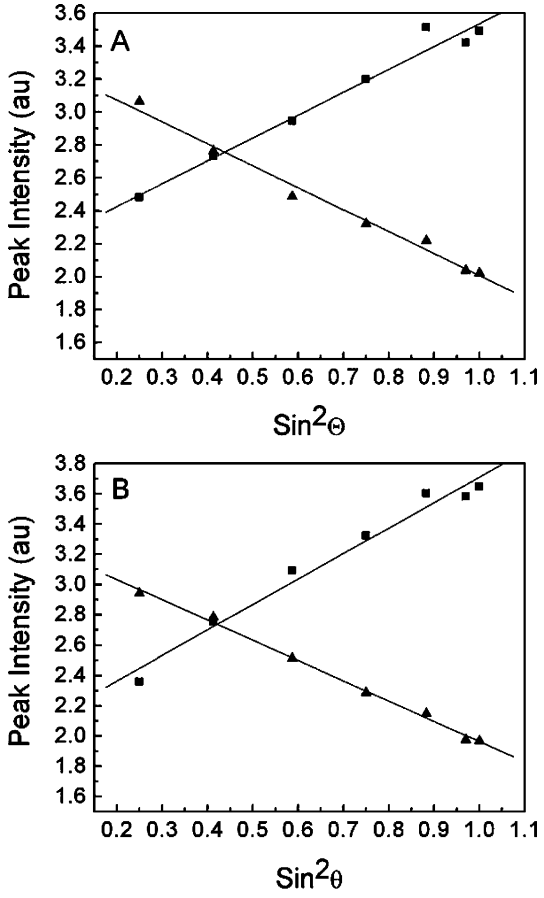


Figure 6. (A, B) Normalized carbon K-edge PEY NEXAFS spectra as a function of sin 2θ for $1s \rightarrow \sigma^*$C−C (▲) and $1s \rightarrow \sigma^*$C−H (■). The linear fits are meant to guide the eye.

Table 2. Calculated Tilt Angles from the NEXAFS Spectra for the Two Different Self-Assembled Monolayers Deposited onto the AZO Thin Films

monolayer	bond	tilt angle (deg)[a]
hexadecanethiol	C−H	50
	C−C	30
	average tilt	40 ± 10
octadecanethiol	C−H	45
	C−C	25
	average tilt	35 ± 10

[a] The tilt angle is defined as the angle formed between the alkyl chain of the SAMs and the normal to the ITO surface.

angle values for the different types of SAMs indicates that the SAMs that formed differ structurally. Thus, although both long-chain thiolates form relatively well-organized, ordered SAMs on AZO, the molecular organization in the two SAMs is different.

The experimental results were complemented by density functional theory (DFT) calculations. These calculations provide a survey of different levels of Al doping and oxygen depletion to estimate the charge carrier density for comparison with the observed plasma frequency (eq 7). As stated earlier, the effect of Al doping is due to the fact that the increased aluminum electron count results in the donation of electron density to the conduction band. Experimentally, Hall effect measurements determined the charge carrier concentration value to be 4.7×10^{20} e/cm^3 for a 2% aluminum-doped zinc oxide thin film. The calculated charge carrier density is 7.0×10^{20} e/cm^3 for 9% Al doping and 18% oxygen depletion, which corresponds to a plasma frequency of 14 700 cm^{-1} (Supporting Information). The screened

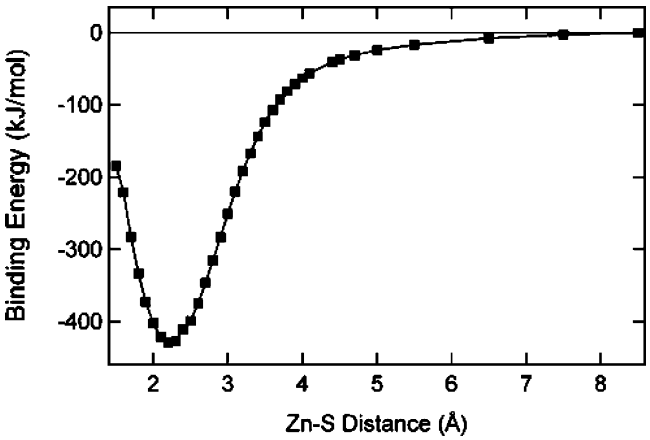


Figure 7. DFT-calculated potential energy curve for a ZnO substrate for the binding of an ethane thiolate SAM using periodic boundary conditions.

surface plasmon frequency, $\omega_{ps} = \omega_p/\sqrt{(1+\epsilon_\infty)}$, is 7100 cm^{-1}, given that ϵ_∞ has a value of 3.24. The calculated value should be compared to an experimentally measured value of $\omega_{ps} = 8500$ cm^{-1}. As observed in previous calculations for IrO_2 and $CdSn_2O_4$,[47,58] the resulting plasma frequencies reveal a strong dependence on the oxygen depletion level in which increased oxygen depletion levels lead to higher-energy plasma frequencies. In AZO, the charge carrier density passes through a maximum as a function of oxygen depletion. The dependence on the Al doping level is not as strong..

DFT investigations of the strength of the zinc−sulfur bond provide further insight into the experimental observations of high surface density and the order of alkane thiolate SAMs. Figure 7 shows the DFT-calculated potential energy curve for a ZnO substrate for the binding of an ethane thiolate SAM using periodic boundary conditions. The ethane thiolate molecules were placed in a $(\sqrt{3} \times 3)R30°$ lattice superimposed on the orthorhombic unit cell of the ZnO substrate. As shown in the Figure, the maximum binding energy is reached at an atomic distance of 2.2 Å, at which point a binding energy of nearly 430 kJ/mol is calculated. For comparison, a comparable ethane alkane thiol layer on gold(111) has been calculated to have a maximum binding energy of ∼160 kJ/mol[70] whereas a hexadecanethiol monolayer on ITO was estimated to have a maximum binding energy of ∼30 kJ/mol.[22] As stated above, the thiolated monolayers appear to be both robust and ordered, thus this calculation provides a possible explanation for some of these observed properties.

Conclusions

This study explores the capacity of aluminum-doped zinc oxide to form well-ordered, reproducible, robust thiolate SAMs as well as an optical response of thin films of AZO. The four methods employed—reflectance FTIR spectroscopy, XPS, contact angle, and NEXAFS spectroscopy—provided complementary information on the formation of adlayers on AZO and afforded a comparison with similar measurements on ITO.[22,61] The order and stability of thiolate adlayers on AZO are both superior to those for the corresponding SAMs on ITO. Optical property studies with FTIR suggest similar optical properties for AZO and ITO, although the deposition conditions of AZO and the stability of the films are characteristic of alkane thiolate SAMs on gold much more than SAMs on ITO. XPS spectra of both ITO and AZO confirmed the presence of a thiolated adlayer through the appearance of a sulfur peak. The contact angle revealed a slightly better packing density on AZO while confirming the inhomogeneity of both surfaces. Further characterization by NEXAFS spectroscopy confirmed the existence of the adlayer and also provided information about the organization and molecular tilt angle of the constructed SAM on the surface. The ordering and tilt angle of the thiolated monolayers on AZO determined from the NEXAFS data are similar to those reported for gold.[69] These results illustrate the diversity of conducting metal oxides with substrates ranging from those, such as AZO, exhibiting properties similar to those of metals to those whose properties more closely resemble those of semiconductors, such as ITO.[71]

A possible explanation for this diversity is the strength of the substrate−sulfur bond, which attaches the thiolated adlayer to the surface. The zinc−sulfur bond in zinc sulfide is related to the indium−sulfur bond.[72,73] In fact, the strength of the interaction of the zinc oxide−sulfur bond is such that immobilized ZnO has been used to scavenge hydrogen sulfide at concentrations ranging from 50 to 20 000 ppmv (parts per million by volume).[72] Hydrothermal vent worms have evolved to use zinc ions to chealate the sulfide ions from hydrogen sulfide in these harsh environments.[73] However, the indium−sulfur bond has been shown to be very weak.[74,75] Experimental evidence has shown that the ITO sulfur bond is extremely dependent on both film thickness and annealing conditions. Moverover, deposition in neat alkane thiolates is required for film reproducibility.[61] DFT calculations of the potential energy curve for the Zn−S bond substantiated that the bond strength is not only stronger than In−S but also stronger than Au−S. The stability of the well-ordered SAMs formed on the AZO is a key advance in efforts to stabilize AZO for electronics and sensing applications.

Acknowledgment. We thank Accelrys, Inc. for access to DFT computing program DMol3. The NEXAFS experiments were performed at the National Synchrotron Light Source at Brookhaven National Laboratory, which is funded by the U.S. Department of Energy, Division of Materials Sciences and Division of Chemical Sciences. The AZO thin films were graciously provided by the National Center for Photovoltaics at the National Renewable Energy Laboratory.

Supporting Information Available: Modeling of the experimental data by the Drude free-electron model and results from density functional theory calculations completed for the AZO thin films. This material is available free of charge via the Internet at http://pubs.acs.org.

LA701741M

(70) Franzen, S. *Chem. Phys. Lett.* **2003**, *381*, 315−321.

(71) Brewer, S.; Franzen, S. *J. Alloys Compds.* **2002**, *343*, 244−244

(72) Lu, Y.; Sathitsuksanoh, N.; Yang, H. Y.; Chang, B. K.; Queen, A. P.; Tatarchuk, B. J. Microfibrous Entrapped ZnO−Support Sorbents for High Contacting Efficiency H_2S Removal from Reformate Streams in PEMFC Applications. In *Microreactor Technology and Process Intensification*; Wang, Y., Holladay, J. D., Eds.; ACS Symposium Series 914; American Chemical Society: Washington, DC, 2005; Vol. 914, pp 406−422.

(73) Flores, J. F.; Fisher, C. R.; Carney, S. L.; Green, B. N.; Freytag, J. K.; Schaeffer, S. W.; Royer, W. E. *Proc. Natl. Acad. Sci. U.S.A.* **2005**, *102*, 2713−2718.

(74) Kale, S. S.; Mane, R. S.; Lokhande, C. D.; Nandi, K. C.; Han, S. H. *Mater. Sci. Eng., B* **2006**, *133*, 222−225.

(75) Kumar, P. M. R.; John, T. T.; Kartha, C. S.; Vijayakumar, K. P.; Abe, T.; Kashiwaba, Y. *J. Mater. Sci.* **2006**, *41*, 5519−5525.